Catalysis Letters
https://doi.org/10.1007/s10562-023-04565-y

A First Principles Mechanistic Study of Higher Alcohol Synthesis from Syngas on a Stepped Rhodium Surface

Ryan Lacdao Arevalo[1] · **Hiroshi Nakanishi**[1,2,3]

Received: 5 October 2023 / Accepted: 18 December 2023

Abstract

The mechanism of higher alcohol synthesis (HAS) from syngas on a stepped Rhodium surface was explored using first principles calculations based on density functional theory. Results showed that the activation of CO proceeds most energetically feasible via a sequential hydrogenation towards CH_2OH, followed by the C–OH bond cleavage yielding CH_x species. Because the initial CO hydrogenation step is highly activated, the cascade of elementary steps toward methane formation is highly favored. The formation of C_2 oxygenates toward ethanol production is kinetically favored by CO insertion to CH_2, or alternatively, by a lower activation barrier CHO insertion to CH_3. On the other hand, the C_3 species is formed more preferably by CO rather than CHO insertion to a CH_3CH_2 fragment, indicating the effect of a more extended carbon structure on the reaction mechanism. The overall reaction mechanism for HAS points to a cycle of CO insertion, hydrogenation, and OH elimination steps.

Graphical Abstract

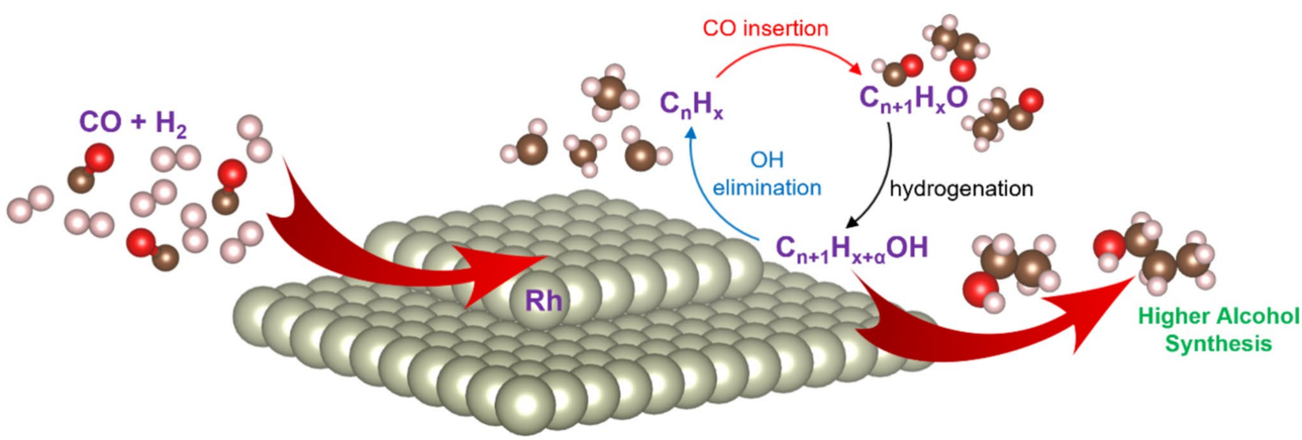

Keywords Higher alcohol synthesis · Rhodium-based catalysts · CO insertion · Density functional theory

✉ Hiroshi Nakanishi
nakanishi@akashi.ac.jp

[1] National Institute of Technology, Akashi College, Nishioka, Uozumi, Akashi, Hyogo 679-3674-8501, Japan

[2] Institute of Industrial Science, The University of Tokyo, Meguro, Tokyo 153-8505, Japan

[3] Institute for NanoScience Design, Osaka University, 2-1 Yamadaoka, Suita, Osaka 565-0871, Japan

1 Introduction

The direct conversion of syngas ($CO+H_2$) into higher alcohols (two or more carbon atoms) is a contemporary challenge in catalysis. Its potential as a sustainable route to manufacturing fuels and valuable chemicals is hindered by low selectivity and product yield of conventional catalysts such as Rh [1–4]. Thus, in the development of active and

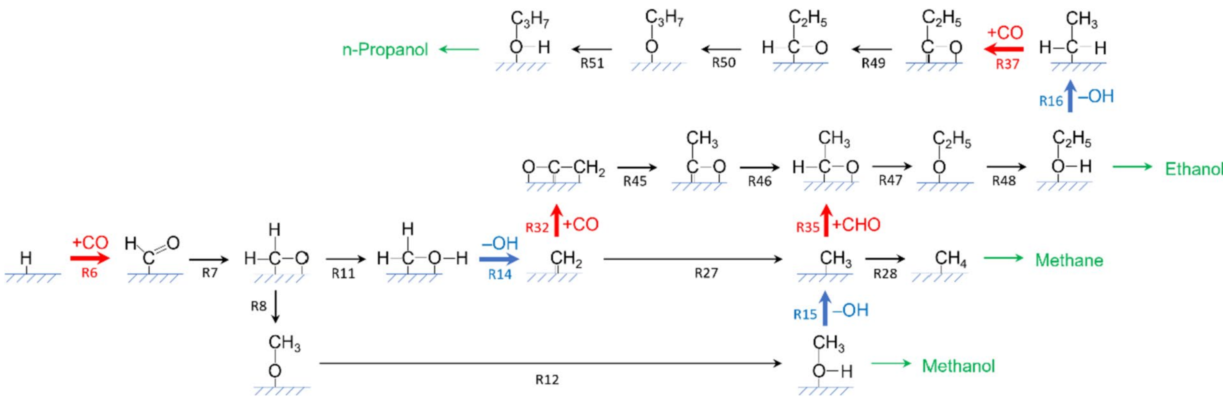

Scheme 1 The proposed reaction mechanism for HAS from syngas on Rh(211). The arrows are color-coded according to the type of elementary steps: desorption (green), hydrogenation (black), C–OH bond cleavage by OH elimination (blue), and CO or CHO insertion (red). Each elementary step is labeled (R1, R2, R3, …) based on Table 1

selective catalysts for this reaction, it is crucial to clarify the reaction mechanism of higher alcohol synthesis (HAS) from syngas on a Rh catalyst. Previous theoretical studies revealed that elementary steps such as hydrogenation, C–C coupling, and C–O bond breaking reactions are relevant to produce the C_2 oxygenates [5–8]. There is a consensus in the literature that the C–C bond of a C_2 species is formed by CH_xO insertion to a CH_x fragment (where x is an integer) [3, 6, 7, 9, 10]. For example, Kapur et al. showed through first principles calculations that ethanol is formed on both the (111) and (211) surfaces of an fcc Rh by CO insertion to a CH_2 fragment [7]. On the other hand, Wang et al. revealed that a more energetically favorable pathway on Rh(211) is via the CHO insertion to CH_3 [6]. While the reaction mechanism for the production of C_2 alcohol was clarified on these studies, the mechanism of the succeeding CH_xO (x = 0, 1) insertion reactions to a C_2 species towards the production of C_3 oxygenates has remained unexplored in theoretical studies. This is important because the insertion of a CH_xO species on a C_2 hydrocarbon involves a more complex reorientation of the C_2H_x species in the formation of the C–C bond with CH_xO. Experimentally, it was shown that a C_3 alcohol (n-propanol) can be produced on a Rhodium catalyst [11]. In the current work, the mechanism for the production of C_2 oxygenates on Rh(211) is first revisited and further extended to the formation of C_3 oxygenates. The explored elementary steps for HAS synthesis include the activation of CO by dissociation and hydrogenation, C–O bond cleavage for the formation of CH_x species from CH_xO, C–C coupling by insertion of CH_xO species to CH_x forming C_2 oxygenates and coupling of CH_x species, and the formation of C_3 oxygenates from C_2 species. To this end, a general scheme for the mechanism of HAS will provide insights into the design and development of catalysts for this reaction.

2 Results and Discussion

As an overview of the results, the identified reaction paths for HAS are shown in Scheme 1. Here, CO is first activated through hydrogenation to form the CHO species, which further hydrogenates into CH_2O and CH_2OH species. Note that in Scheme 1, the hydrogenation of CO is depicted as an equivalent reaction of CO insertion to an H adatom. CH_2OH dissociates yielding CH_2, which easily hydrogenates into CH_3 and CH_4. Methanol is produced by the hydrogenation of CH_2O into CH_3O and further into CH_3OH. The insertion of CO is more preferred in CH_2 than in CH_3, albeit the CHO insertion to CH_3 has a lower activation barrier than the CO insertion to CH_2. Further hydrogenation of C_2 species from these insertion steps forms ethanol. Meanwhile, an OH elimination step can form the CH_3CH_2 species, which can be converted to n-propanol by CO insertion and subsequent hydrogenation steps. The details of this identified reaction mechanism are discussed in the following sections. The activation barriers for different elementary steps are shown in Table 1. While there are many other possible elementary steps involved in the overall HAS, Table 1 only shows the relevant elementary steps based on the calculated activation barriers (i.e., low-barrier steps).

2.1 CO Activation: Dissociation Versus Hydrogenation

In the HAS reaction from syngas, the activation of CO via dissociation or hydrogenation determines the mechanistic route to produce alcohol and other products such as methane, CO_2, and other hydrocarbons. The dissociation of CO into C and O adatoms has been proposed to

Table 1 The calculated activation barriers E_a and reaction energies ΔE for relevant elementary steps. The symbols ΔG_a and ΔG are the corresponding Gibbs free energy barriers and reaction free energies, respectively, evaluated at temperature T = 300 K

	Reactions	E_a (eV)	ΔE (eV)	ΔG_a (eV)	ΔG (eV)
(a) C–O bond dissociation					
R1	$CO \rightarrow C + O$	3.61	0.86	3.54	0.85
R2	$CO + H \rightarrow C + OH$	2.70	1.00	2.61	1.10
R3	$CHO \rightarrow CH + O$	1.94	0.18	1.88	0.14
R4	$CH_2O \rightarrow CH_2 + O$	1.69	–0.11	1.62	–0.17
R5	$CH_3O \rightarrow CH_3 + O$	1.38	–0.24	1.23	–0.31
(b) C–H bond formation					
R6	$CO + H \rightarrow CHO$	1.33	1.02	1.35	1.18
R7	$CHO + H \rightarrow CH_2O$	0.79	0.42	0.71	0.49
R8	$CH_2O + H \rightarrow CH_3O$	0.24	0.05	0.25	0.25
(c) O–H bond formation					
R9	$CO + H \rightarrow COH$	1.85	0.89	1.74	1.00
R10	$CHO + H \rightarrow CHOH$	1.55	0.29	1.40	0.44
R11	$CH_2O + H \rightarrow CH_2OH$	0.53	0.03	0.61	0.21
R12	$CH_3O + H \rightarrow CH_3OH$	1.22	0.57	1.09	0.62
(d) CH_x–OH bond dissociation					
R13	$CHOH \rightarrow CH + OH$	1.47	–0.24	1.37	1.29
R14	$CH_2OH \rightarrow CH_2 + OH$	0.96	–0.48	0.84	–0.56
R15	$CH_3OH \rightarrow CH_3 + OH$	1.79	–0.96	1.66	–0.97
R16	$CH_3CH_2OH \rightarrow CH_3CH_2 + OH$	0.93	–0.70	0.78	–0.80
(e) CH production					
R17	$CO + H \rightarrow CH + O$	1.45	1.11	1.43	1.22
R18	$CHO \rightarrow CH + O$	1.94	0.18	1.88	0.14
R19	$CHO + H \rightarrow CH + OH$	1.68	0.13	1.56	0.14
R20	$C + H \rightarrow CH$	0.84	0.07	0.73	–0.04
(f) CH_2 production					
R21	$CHO + H \rightarrow CH_2 + O$	3.25	0.31	3.05	0.35
R22	$CH_2O \rightarrow CH_2 + O$	1.69	–0.11	1.62	–0.17
R23	$CH + H \rightarrow CH_2$	1.09	0.52	0.97	0.40
(g) CH_3 production					
R24	$CH_2O + H \rightarrow CH_3 + O$	1.57	–0.41	1.53	–0.36
R25	$CH_3O + H \rightarrow CH_3 + OH$	1.75	–0.39	1.60	–0.36
R26	$CH_3O \rightarrow CH_3 + O$	1.38	–0.24	1.23	–0.31
R27	$CH_2 + H \rightarrow CH_3$	0.51	0.10	0.42	0.03
R28	$CH_4 \rightarrow CH_3 + H$	0.25	–0.32	0.15	–0.41
(h) CH_x–CH_x coupling					
R29	$CH_3 + CH_3 \rightarrow C_2H_6$	1.76	0.08	1.55	0.20
R30	$CH_2 + CH_2 \rightarrow C_2H_4$	1.59	–0.30	1.51	–0.20
R31	$CH + CH \rightarrow C_2H_2$	4.18	0.21	4.18	0.24
(i) CH_xO insertion					
R32	$CH_2 + CO \rightarrow CH_2CO$	1.11	0.84	1.12	0.90
R33	$CH_2 + CHO \rightarrow CH_2CHO$	0.72	–0.36	0.70	–0.31
R34	$CH_3 + CO \rightarrow CH_3CO$	1.51	0.63	1.51	0.71
R35	$CH_3 + CHO \rightarrow CH_3CHO$	0.58	–0.24	0.60	–0.16
R36	$CH_3 + CH_2O \rightarrow CH_3CH_2O$	1.78	–0.07	1.86	0.10
R37	$CH_3CH_2 + CO \rightarrow CH_3CH_2CO$	1.38	0.34	1.32	0.33
R38	$CH_3CH_2 + CHO \rightarrow CH_3CH_2CHO$	1.97	–0.12	1.81	–0.06
(j) OH reactions and CO oxidation					
R39	$OH \rightarrow H + O$	1.33	0.19	1.08	0.30
R40	$OH + H \rightarrow H_2O$	1.63	0.42	1.59	0.53
R41	$CO + O \rightarrow CO_2$	1.72	0.49	1.70	0.51

Table 1 (continued)

	Reactions	E_a (eV)	ΔE (eV)	$ΔG_a$ (eV)	ΔG (eV)
R42	CO + OH → COOH	1.97	0.81	1.85	0.86
R43	CO + OH → CO_2 + H	2.85	0.88	2.61	0.76
R44	CO + OH → HCOO	4.49	0.61	4.22	0.60
(k) Hydrogenation of C_2 and C_3 species					
R45	CH_2CO + H → CH_3CO	0.58	–0.19	0.58	–0.07
R46	CH_3CO + H → CH_3CHO	1.04	0.56	1.09	0.62
R47	CH_3CHO + H → CH_3CH_2O	0.51	–0.03	0.54	0.15
R48	CH_3CH_2O + H → CH_3CH_2OH	1.36	0.50	1.16	0.59
R49	CH_3CH_2CO + H → CH_3CH_2CHO	0.73	0.35	0.71	0.40
R50	CH_3CH_2CHO + H → $CH_3CH_2CH_2O$	0.53	0.05	0.55	0.25
R51	$CH_3CH_2CH_2O$ + H → $CH_3CH_2CH_2OH$	1.26	0.45	1.21	0.61

be the initial step to produce CH_4 and CH_3CH_2OH (ethanol) [7]. CO adsorbs at the bridge-edge site of Rh(211) and dissociates, as shown in Fig. 1a. However, CO dissociation on Rh(211) requires a large activation barrier of 3.61 eV, which is consistent with other DFT studies on other surfaces such as Co(0001) [9] and Rh(111) [5.7–8]. Although the calculation of hydrogen-assisted C–O bond dissociation (CO + H → C + OH, R2) revealed a lower energy barrier of 2.70 eV, the kinetics is still expected to be slow. In contrast, the calculated activation barrier for CO hydrogenation (CO + H → CHO, R6) is 1.33 eV, consistent with a previous DFT study [6]. This indicates a strong kinetic preference for CO hydrogenation rather than dissociation, which is supported by studies that reported CO hydrogenation as the dominant pathway for alcohol production, such as methanol and ethanol [5, 6,

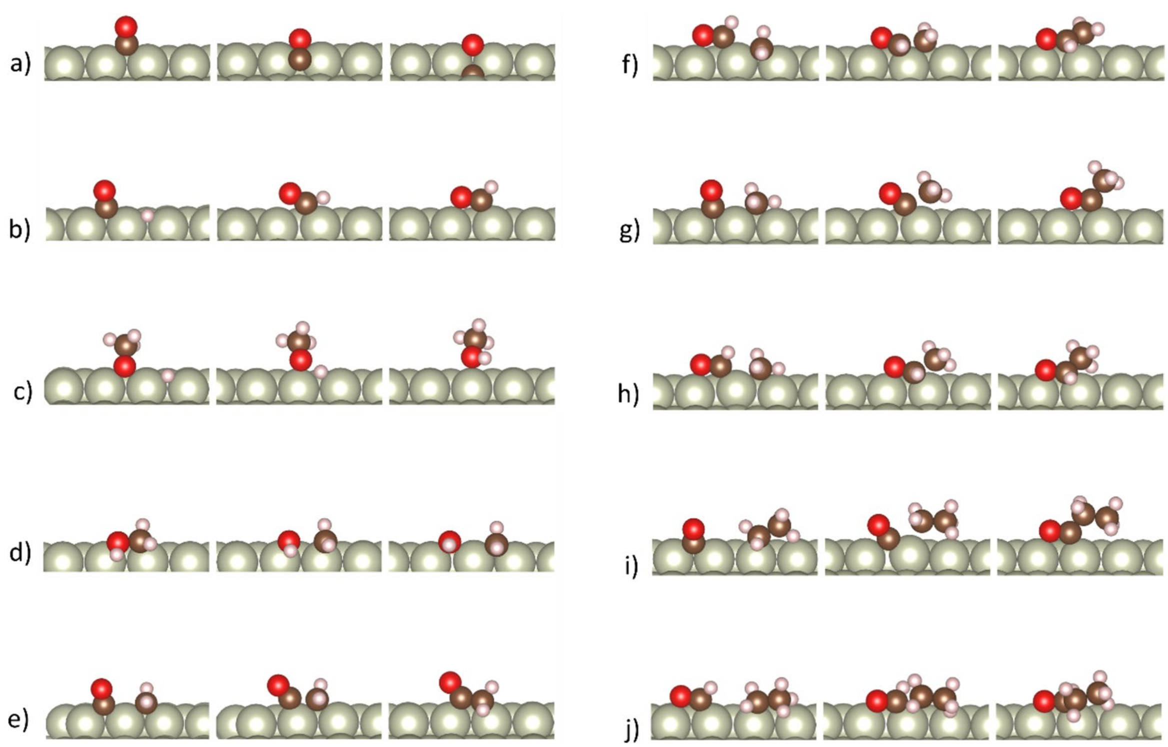

Fig. 1 The initial (left), transition (middle), and final (right) states of some key elementary steps on Rh(211): (**a**) CO → C + O (R1), (**b**) CO + H → CHO (R6), (**c**) CH_3O + H → CH_3OH (R12), (**d**) CH_2OH → CH_2 + OH (R14), (**e**) CH_2 + CO → CH_2CO (R32), (**f**) CH_2 + CHO → CH_2CHO (R33), (**g**) CH_3 + CO → CH_3CO (R34), (**h**) CH_3 + CHO → CH_3CHO (R35), (**i**) CH_3CH_2 + CO → CH_3CH_2CO (R37), (**j**) CH_3CH_2 + CHO → CH_3CH_2CHO (R38). The red, brown, pink, and gray colors denote the O, C, H, and Rh atoms, respectively. In these figures, the < 111 > plane is directed upward. The figures for the other elementary steps are shown in the Supplementary Information

8]. Meanwhile, the hydrogenation of CO into COH (O–H bond formation) requires an activation barrier of 1.85 eV, which is higher than its hydrogenation into CHO. This implies that the C–H bond formation is easier compared to O–H bond formation for the first hydrogenation of CO. In this regard, the subsequent elementary steps considered are the pathways via the CHO as an intermediate species (herein referred to as the CHO-pathway).

Subsequent hydrogenation (C–H bond formation) steps from CHO to CH_2O and CH_3O require lower activation barriers of 0.79 eV and 0.24 eV, respectively. These results suggest that while the initial hydrogenation of CO is kinetically challenging, the subsequent hydrogenation steps are more facile. This is consistent with a previous study identifying the initial hydrogenation of CO into CHO as the rate-determining step in the hydrogenation pathway of CO into ethanol [5]. As shown in Fig. 1b, the initial hydrogenation of CO into CHO requires a high activation energy because the CO molecule must tilt from its bidentate adsorption configuration into a monodentate structure at the transition state. Nevertheless, the activation barriers for the sequential hydrogenation of CO are still much lower than its direct dissociation into atomic carbon (CO → C + O, R1).

To assess the impact of hydrogenation on C–O bond cleavage, the dissociation barriers were calculated for the CH_xO species. Results showed that the C–O bond dissociation barriers decrease and the reaction energies become more exothermic as the number of hydrogen atoms x in the CH_xO species increases (Table 1a). This indicates that the C–O bond of a CH_xO species is weakened by hydrogenation. This is consistent with other DFT studies, that identified the significant lowering of the C–O dissociation barrier by hydrogenation [5, 6, 8].

The formation of an O–H bond in the CH_xO species is important for the formation of the hydroxyl group in an alcohol. The increasingly hydrogenated CH_xO species (CO → CHO → CH_2O) has a decreasing trend of activation barriers and lesser endothermic reaction energies for O–H bond formation (Table 1c). The lowest activation barrier (0.53 eV) is for the hydrogenation of CH_2O into CH_2OH. However, the hydrogenation of CH_2O into CH_3O has a lower barrier of 0.24 eV, which implies that a C–H bond formation is more likely than the O–H bond formation for CH_2O. It can be noted that the O–H bond formation for CH_3O to produce CH_3OH (methanol) requires a large activation barrier of 1.22 eV as the CH_3O species must break loose the O–Rh bonds as it transitions from the bidentate to monodentate adsorption configuration (Fig. 1c).

2.2 Formation of CH_x Species

In the CHO-pathway, CH can form via the hydrogen-assisted dissociation of CO (CO + H → CH + O, R17), dissociation of CHO (CHO → CH + O, R18), or hydrogen-assisted dissociation of CHO (CHO + H → CH + OH, R19). Among these reactions, the hydrogen-assisted dissociation of CO requires the lowest activation barrier equal to 1.45 eV. It can be noted that the CH formation by hydrogenation of C only requires an activation barrier of 0.84 eV, but it is unlikely to have surface adsorbed C reactants because of the earlier mentioned high activation barrier for CO dissociation. For CH_2 formation via the CHO-pathway, CH_2 can be produced via the hydrogenation of CH with an activation barrier of 1.09 eV, but such reaction is unlikely because of the large barriers for CH formation in the CHO-pathway. Meanwhile, CH_2 formation from the dissociation of CH_2OH into CH_2 and OH requires the lowest activation barrier of 0.96 eV. On the other hand, CH_3 can be formed most favorably from the hydrogenation of CH_2. Based on these calculations, the pathway towards the formation of CH_x species that requires the lowest activation barrier is CO → CHO → CH_2O → CH_2OH → CH_2 → CH_3 → CH_4.

In this pathway toward the formation of methane (CH_4), the elementary step that requires the highest activation barrier is the initial hydrogenation of CO. This indicates that once the initial hydrogenation of CO is achieved, the subsequent steps toward the formation of methane is facile. Experimentally, it was shown that a large amount of methane is produced in the HAS from syngas on Rh, which limits the desired production of higher alcohols [11].

Note that in the formation of a CH_2 species, OH is eliminated through the dissociation of CH_2OH (Fig. 1d). The adsorbed OH species can react with hydrogen adatoms to produce H_2O, or dissociate into H and O. The calculation of energy barriers for these elementary steps showed that OH prefers to dissociate rather than to form H_2O (Table 1j). In this regard, the O adatoms that are produced from the dissociation of OH can oxidize the surface CO adsorbates yielding CO_2 gas. The calculated activation barrier for the oxidation of CO is 1.72 eV, which is slightly higher than for the hydrogenation of CO. Experimentally, a small amount of CO_2 has been detected in the HAS from syngas on Rh [11].

2.3 C_2 Formation: CO Insertion vs CHO Insertion

As mentioned in the previous Section, the CH_2 and CH_3 species are the relevant CH_x species before the formation of methane. The subsequent production of C_2-species can proceed via the CH_x-CH_y coupling or the insertion of a CH_xO species in a CH_x fragment. Calculations revealed large activation barriers for the CH_x-CH_y coupling reactions on Rh(211) (Table 1h). This is consistent with another DFT study that reported high barriers for producing C_2 hydrocarbons via CH_x–CH_y coupling on Rh [12]. In this regard, the C–C coupling reactions via the insertion of CH_xO species to CH_2 and CH_3 were calculated. Results showed that for the case of CH_2, the insertion of CHO promotes lower activation barrier and more exothermic reaction energy than for CO insertion. Figure 1e, f shows the initial, transition, and final states for these reactions. A high activation barrier of 1.11 eV is required for CO insertion to CH_2 as similarly noted for CO hydrogenation into CHO because of the change of the CO adsorption configuration from a bidentate C–Rh interaction at the initial state into a monodentate C–Rh binding at the transition state. On the other hand, the CHO insertion requires a lower activation barrier of 0.72 eV and a more exothermic reaction energy. For this reaction, the CHO molecule has a favorable initial adsorption configuration to facilitate a facile binding with CH_2. Such trend was also observed for the case of CO and CHO insertion to CH_3. As shown in Table 1i, CHO insertion to CH_3 requires a lower activation barrier and more exothermic reaction energy than CO insertion. Similar to the case of CO and CHO insertion to CH_2, a lower activation barrier for CHO insertion than for CO insertion is due to the favorable initial adsorption configuration of CHO that facilitates a facile reaction with CH_3 (Fig. 1g, h). Among the CH_xO insertion reactions with CH_2 and CH_3, the lowest activation barrier is achieved by CHO insertion to CH_3. However, in an environment with abundant CO molecules, the CO insertion reaction is more favorable for CH_2 than for CH_3. This indicates that the reaction mechanism to produce C_2 oxygenates depends highly on the presence of oxidants CO or CHO. That is, C_2 oxygenates are either produced via CO insertion to CH_2 in a CO-abundant environment, or via the CHO insertion to CH_3 in the presence of high quantities of CHO. These observations agree with the previous works of Kapur et al. and Wang et al., [6, 7] which identified either CH_2 or CH_3 as intermediates for ethanol formation. Nevertheless, the hydrogenation of CH_2 to produce CH_3 is still more kinetically favored than the CO insertion reaction to CH_2, which explains the experimentally observed high methane quantities produced in HAS on Rh [11].

2.4 C_3 Formation

After the formation of a C_2 oxygenate, further hydrogenation steps towards the production of ethanol (CH_3CH_2OH) require the highest activation barrier of 1.36 eV, in agreement with a previous DFT study [6]. Ethanol can desorb from the surface with a desorption energy of 1.02 eV, or dissociate into $CH_3CH_2 + OH$ with an activation barrier of 0.93 eV. The production of C_3 oxygenates is proposed to proceed via CO or CHO insertion to CH_3CH_2. Calculations showed that CO insertion is more favored than CHO insertion, unlike the cases of CH_2 and CH_3 that prefer the CHO insertion reaction (Table 1i). This indicates the effect of a more extended C_2 hydrocarbon structure in the CO or CHO insertion reaction. For CHO insertion in both monocarbon CH_2 or CH_3 and dicarbon CH_3CH_2 (Fig. 1i, j), the hydrocarbon fragment must detach from the surface to form a new C–C bond with CHO. This step costs a larger amount of energy for a more extended C_2 structure than a C_1 fragment. Thus, CH_3CH_2CO rather than CH_3CH_2CHO is predicted to be the first C_3 species that can be produced in the investigated sequence of carbon chain growth. This may indicate that, contrary to the production of a C_2 alcohol, CO insertion is more favorable than CHO insertion for the production of higher alcohols (>C_2). Further hydrogenation of CH_3CH_2CO into n-propanol ($CH_3CH_2CH_2OH$) requires the highest activation barrier of 1.26 eV, which is lower than the activation barrier for CO insertion to CH_3CH_2. This shows that the possible limiting step to produce a C_3 species is the CO insertion reaction to a C_2 species.

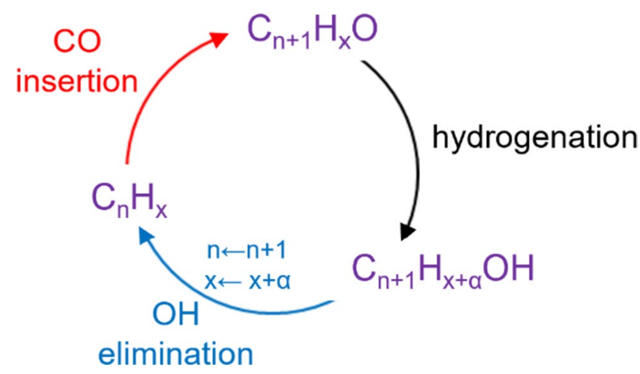

Scheme 2 The overall reaction cycle for HAS consisting of CO insertion (red), hydrogenation (black), and OH elimination (blue)

A general scheme for this overall reaction mechanism is shown in Scheme 2. Here, the overall reaction cycle is facilitated by a series of CO insertion to a C_nH_x species, hydrogenation of a $C_{n+1}H_xO$ oxygenate into a $C_{n+1}H_{x+\alpha}OH$ alcohol (where $\alpha + 1$ denotes the number of added hydrogen atoms), and an OH elimination step to form a new hydrocarbon. The reaction starts with $n = 0$ for an adsorbed H, then CO insertion to form a CHO species, which further hydrogenates to produce methanol or CH_2OH, which can undergo an OH elimination reaction to form a CH_x species. The reaction continues with another CO insertion, followed hydrogenation to form an alcohol, and so on.

While the current study provides a fundamental insight into the mechanism of alcohol synthesis on a conventional catalyst, recent advances in catalyst design revealed that the catalyst selectivity toward higher alcohol synthesis can be tuned by modifying the catalyst composition and morphology, [13–15] as well the introduction of promoters and support effects [16]. Nevertheless, the current study highlights the importance of promoting a facile CO insertion reaction in catalyst design, as well as the roles of the hydrogenation and OH elimination steps in the carbon chain growth for the synthesis of higher alcohols.

3 Conclusion

Density functional theory-based calculations revealed the reaction mechanism for higher alcohol synthesis from syngas on Rh(211). Upon the initial adsorption of the CO molecule on the surface, the energetically preferred CO activation is via the hydrogenation reaction yielding a CHO species rather than through the direct dissociation of the C–O bond. The C–O bond is weakened by hydrogenation, resulting in the production of CH_x species. Subsequent to the initial hydrogenation of CO to CHO, the elementary steps toward the production of CH_4 proceed kinetically facile, which explains the experimentally determined large methane production that limits the synthesis of higher alcohols on Rhodium-based catalysts. The C_2 species can be formed by CO insertion to CH_2, or by CHO insertion to CH_3, with the latter having a lower activation barrier. Meanwhile, the C_3 species can be formed by CO insertion to a CH_3CH_2 fragment, which is more energetically favored than CHO insertion. These results provide the reaction mechanism for higher alcohol synthesis, which points to the importance of promoting a more facile CO insertion to enhance the selectivity of Rh-based catalysts for this reaction, as well as the roles of the hydrogenation and OH elimination steps in the carbon chain growth for the formation of higher alcohols.

Computational Model An fcc bulk Rh was modelled using a cubic supercell with four Rh atoms at the following fractional coordinates: (0,0,0), (0, 0.5, 0.5), (0.5, 0, 0.5), and (0.5, 0.5, 0). The lattice constant was calculated by relaxing the ions and volume of the supercell using the conjugate gradient algorithm [17] to within a force tolerance of 0.001 eV/ Å. The surface Brillouin zone integrations were performed on a grid of 8 × 8 × 8 Monkhorst–Pack k-points [18] using Methfessel – Paxton smearing [19] of σ = 0.2 eV, and energy cut-off of 500 eV. The interaction between ions and electrons was described using the projector augmented wave (PAW) method [20, 21]. Spin-polarized density functional theory (DFT) calculations were carried out using the Vienna ab initio simulation package (VASP) [22–25].

Table S1 shows the calculated lattice constants for different DFT functionals. For comparison, the experimentally determined [26] lattice constant is also shown. It can be noted from the table that the obtained lattice constant using the DFT method within the generalized gradient approximation (GGA) based on the Perdew–Burke–Ernzerhof (PBE) functional [27–30] with van der Waals correction (D3) by Grimme [31] is closest to the experimental value. Such functional was used for all the subsequent calculations.

The stepped surface of an fcc Rh was modeled using a (211) surface in a 4 × 1 supercell (Fig. S2) with thickness equivalent to four atomic layers of the (111) facet and vacuum space of ca. 12.0 Å. The calculation of adsorption energies for the biggest molecule explored in the study (n-propanol) using a 4 × 1 and a 4 × 2 supercell showed an energy difference of only 0.014 eV (Fig. S3). Furthermore, the total energy of the n-propanol-slab system changed by only 0.04 eV as the vacuum space is increased from 12.0 Å to a much larger 20.0 Å. The total energies for the vacuum-slab model were calculated using a 500-eV energy cut-off and 6 × 5 × 1 Monkhorst Pack k-points. An electric dipole correction in the z-direction was used to cut the spurious interaction between the repeated images of the slab model. The gas-phase molecules were modelled using one free molecule inside a 20 × 20 × 20 $Å^3$ supercell with electric dipole correction implemented in all directions. The optimal adsorption configuration of molecules on the (211) surface was identified by exploring several possible orientations of the molecules at the different sites on the surface. The transition states for elementary steps were identified using the Climbing Image Nudged Elastic Band method [32] and Dimer Method [33]. The activation barriers E_a for the elementary steps are calculated by getting the difference in the total energies of the transition state and initial state. Similarly, the reaction energies ΔE are calculated by subtracting the total energy of the initial state from the final state. A negative value for ΔE implies an exothermic reaction. For comparison, the effect of temperature on the elementary steps are considered by adding the vibrational contributions using the Helmholtz free energy $F_{vib}(v_i, T)$, to the DFT-calculated total energy, as discussed in our previous works [34–36]:

$$F_{vib}(v_i, T) = E_{ZPVE} + \Delta E_{vib,0\rightarrow T} - S_{vib}T = 1/2 \sum_i \left\{ hv_i + 2k_B T ln \left[1 - exp\left(-\frac{hv_i}{k_B T} \right) \right] \right\} \quad (1)$$

Here, the terms E_{ZPVE}, $\Delta E_{vib,0\rightarrow T}$, and $S_{vib}T$ are the zero-point vibrational energy, vibrational energy change for temperature increase from 0 to T K, and the vibrational entropy, evaluated at temperature T = 300 K. The symbols h, k_B, v_i, and T, are the Planck's constant, the Boltzmann constant, harmonic vibrational frequency, and temperature, respectively. The corresponding Gibbs free energies for the barriers ΔG_a and reaction energies ΔG are shown in Table 1. It can be noted that while the inclusion of the energy correction changes the barriers to a maximum of 0.20 eV, the proposed reaction mechanism for higher alcohol synthesis remains the same.

Supplementary Information The online version contains supplementary material available at https://doi.org/10.1007/s10562-023-04565-y.

Acknowledgements This work is supported by the Ministry of the Environment, Government of Japan, through the "Demonstration

Project of Innovative Catalyst Technology for Decarbonization through Regional Resource Recycling".

Funding The Ministry of the Environment, Government of Japan

Declarations

Conflict of Interest All authors declare that they have no conflict of interest.

References

1. Suvarna M, Preikschas P, Perez-Ramirez J (2022) ACS Catal 12:15373
2. Ao M, Pham GH, Sunarso J, Tade MO, Liu S (2018) ACS Catal 8:7025
3. Mei D, Rousseau R, Kathmann SM, Glezakou VA, Engelhard MH, Jiang W, Wang C, Gerber MA, White JF, Stevens DJ (2010) J Catal 271:325
4. Gao J, Mo XH, Goodwin JG (2009) J Catal 268:142
5. Choi Y, Liu P (2009) J Am Chem Soc 131:13054
6. Wang J, Liu Z, Zhang R, Wang B (2014) J Phys Chem C 118:22691
7. Kapur N, Hyun J, Shan B, Nicholas JB, Cho K (2010) J Phys Chem C 114:10171
8. Yang N, Medford AJ, Liu X, Studt F, Bligaard T, Bent SF, Norskov JK (2016) J Am Chem Soc 138:3705
9. Zhuo M, Tan KF, Borgna A, Saeys M (2009) J Phys Chem C 113:8357
10. Schweicher J, Bundhoo A, Kruse N (2012) J Am Chem Soc 134:16135
11. Xu D, Zhang H, Ma H, Qian W, Ying W (2017) Catal Comm 98:90
12. Filot IAW, Broos RJP, van Rijn JPM, van Heugten GJHA, van Santen RA, Hensen EJM (2015) ACS Catal 9:5453
13. Birdja Y, Perez-Gallent E, Figueiredo M, Gottle A, Calle-Vallejo F, Koper M (2019) Nat Energy 4:732
14. Wang D, Qin R, Qui Y, Liu C (2023) Mol Catal 547:113340
15. Gao Y, Shi L, Li S, Ren Q (2020) Phys Chem Chem Phys 22:5070
16. Luk H, Mondelli C, Ferre D, Stewart J (2017) Perez-Ramirez J 46:1358
17. Stich I, Car R, Parrinello M, Baroni S (1989) Phys Rev B 39:4997
18. Monkhorst H, Pack J (1976) Phys Rev B 13:5188
19. Methfessel M, Paxton A (1989) Phys Rev B 470:3616
20. Blochl P (1994) Phys Rev B 50:17953
21. Kresse G, Joubert J (1999) Phys Rev B 59:1758
22. Kresse G, Furthmuller J (1996) Phys Rev B 54:11169
23. Kresse G, Furthmuller J (1996) Comput Mater 6:15
24. Kresse G, Hafner J (1993) Phys Rev B 47:558
25. Kresse G, Hafner J (1994) Phys Rev B 49:14251
26. Arblaster JW (1997) Platin Met Rev 41:184
27. Perdew J, Burke K, Ernzerhof M (1996) Phys Rev Lett 77:3865
28. Perdew J, Burke K, Wang Y (1996) Phys Rev B 54:16533
29. Becke A (1998) Phys Rev A 38:3098
30. Lee C, Yang W, Parr R (1988) Phys Rev B 37:785
31. Grimme S (2004) J Comp Chem 25:1463
32. Henkelman G, Uberuaga BP, Jonsson H (2000) J Chem Phys 113:9901
33. Henkelman G, Jonsson H (1999) J Chem Phys 11:7010
34. Arevalo RL, Escano MCS, Kasai H (2013) ACS Catal 3:3031
35. Arevalo RL, Aspera SM, Escano MCS, Nakanishi H, Kasai H (2017) ACS Omega 2:1295
36. Arevalo RL, Aspera SM, Nakanishi H (2019) Catal Sci Technol 9:232